



**HAL**  
open science

# METALLURGY, HRTEM, MAGNETIC-PROPERTIES AND SPECIFIC-HEAT OF TL<sub>2</sub>BA<sub>2</sub>CU<sub>1</sub>O<sub>6</sub>+DELTA 90 K-SUPERCONDUCTORS OBTAINED BY A NEW PROCESS

Christine Opagiste, M. Couach, A.F. Khoder, T. Graf, A. Junod, G. Triscone, J.  
Muller, T.K. Jondo, J. -L. Jorda, R. Abraham, et al.

## ► To cite this version:

Christine Opagiste, M. Couach, A.F. Khoder, T. Graf, A. Junod, et al.. METALLURGY, HRTEM, MAGNETIC-PROPERTIES AND SPECIFIC-HEAT OF TL<sub>2</sub>BA<sub>2</sub>CU<sub>1</sub>O<sub>6</sub>+DELTA 90 K-SUPERCONDUCTORS OBTAINED BY A NEW PROCESS. *Physica C: Superconductivity and its Applications*, 1993, 205 (3-4), pp.247-258. <10.1016/0921-4534(93)90389-8>. <hal-00569528>

**HAL Id: hal-00569528**

**<https://hal.science/hal-00569528v1>**

Submitted on 26 Feb 2011

HAL is a multi-disciplinary open access archive for the deposit and dissemination of scientific research documents, whether they are published or not. The documents may come from teaching and research institutions in France or abroad, or from public or private research centers.

L'archive ouverte pluridisciplinaire HAL, est destinée au dépôt et à la diffusion de documents scientifiques de niveau recherche, publiés ou non, émanant des établissements d'enseignement et de recherche français ou étrangers, des laboratoires publics ou privés.



HAL Authorization

# Metallurgy, HRTEM, magnetic properties and specific heat of $Tl_2Ba_2Cu_1O_{6+x}$ 90K - superconductors obtained by a new process

**C. Opagiste, M. Couach and A.F. Khoder**

*Centre d'Etudes Nucléaires de Grenoble/SPSMS/LCP, BP 85 X, F-38041 Grenoble Cedex, France*

**T. Graf, A. Junod, G. Triscone and J. Muller**

*Département de Physique de la Matière Condensée, 24 Quai E.-Ansermet, Université de Genève, CH-1211 Genève 4, Switzerland*

**T.K. Jondo, J.-L. Jorda, R. Abraham, M.Th. Cohen-Adad and L.A. Bursill 1**

*Laboratoire de Physico-chimie Minérale II, Université Claude Bernard Lyon I, F-69622 Villeurbanne Cedex, France*

**O. Leckel and M.G. Blanchin**

*Laboratoire de Physique des Matériaux, Université Claude Bernard Lyon I, F-69622 Villeurbanne Cedex, France*

## Abstract:

High-quality  $Tl_2Ba_2CuO_{6+x}$  (2201) compounds were synthesized using a high-pressure route. Starting from  $Tl_2Ba_2O_5$  and CuO, the reactions yielding either the orthorhombic or the tetragonal (superconducting) phases were carried out under 100 bar of oxygen or argon and helium, respectively. Preferential thallium losses are prevented and high sintering temperatures can be used to obtain pure samples with large 2201 grains. The experiments performed include metallographic examinations, X ray diffraction, microprobe analysis, plasma emission spectroscopy, HRTEM, AC susceptibility, Meissner field cooling, hysteresis loops, normal-state susceptibility and specific heat measurements.

## 1. Introduction

The physical properties of the high- $T_c$  cuprates often depend critically on the precise conditions of synthesis. This fact is particularly evident in the case of the  $Tl_2Ba_2CuO_{6+x}$  (2201) system, since two related but distinct phases are stable: the orthorhombic, metallic but non-superconducting phase and the tetragonal superconducting phase with  $T_c$  varying from 0 to 90 K according to the degree of oxidation. Oxidation and thallium losses in the course of the reaction process appear as the main parameters to be controlled if one aims at improving the quality as characterized by phase purity, compositional homogeneity and grain size. Due to the volatility of  $Tl_2O_3$ , thallium losses occur during the 2201 compound formation at atmospheric pressure [ 1] and the reaction temperature has to be kept low. A new route of preparation under high pressure, in the 100 bar range, and at high temperature ( 850-

930 ° C) allows us to easily obtain high-quality polycrystalline samples.

## 2. Sample preparation

Previous investigations by Jorda et al. [ 1,2 ] have shown that the congruent melting oxide  $Tl_2Ba_2O_5$  is a convenient starting material to produce the 2201 compounds. We used  $Tl_2Ba_2O_5$  and CuO (Cerac, 99.9%) powder either directly (batch B) or after annealing for 3 days at 750°C under 1 bar  $O_2$  (batch A). After pressing the stoichiometric mixture under 5 kbar, the pellets were given appropriate heat treatments, i.e.

- (1) reaction at 900-930°C under 100 bar of oxygen during 30 min to obtain the orthorhombic, non-superconducting phase. The weight loss is somewhat below 0.8%;
- (2) reaction at 850°C under 100 bar or argon or helium during 12 min, followed by regrinding and repeating the procedure twice, to form the tetragonal superconducting 2201 phase. A more

significant weight loss of 1.5% is observed in this case.

### 3. HRTEM

The following observations were made in order to characterize the defect structures of various preparations and thereby guide improvements in elaboration techniques. More fundamentally, we attempt to understand why  $Tl_2Ba_2Cu_1O_{6+x}$  may exhibit superconducting transition temperatures over the range 0-90 K, depending on the sample preparation.

Electron microscopic observations were made using a JEOL-200CX instrument operating at 200 keV. The objective lens pole pieces allowed interpretable atomic resolution of 0.23 nm to be achieved for very thin crystals (say  $\sim < 10$  nm). A double-tilt goniometer was used, with tilt range limited to  $+ 10^\circ$ .

Figures 1 (a) and (b) compare typical HRTEM images of one orthorhombic (12E-7) and one tetragonal (12EA-0) sample. The degree of crystalline order and perfection was quite remarkable, compared with earlier preparations at 1 atm [ 1 ].

Virtually no extended defects such as intergrowths of adjacent phases, dislocations or twin boundaries were found. Small traces of an amorphous or poorly crystalline material were found, only rarely, attached to the surface of the tetragonal phase. Perhaps not surprisingly, there was no gross difference between the structure images of the two phases, since the atomic coordinates and site occupancies are not significantly different. Computer simulations of the HRTEM images were achieved without difficulty using published crystallographic data [ 3 ]. This allowed the  $CuO_2$  sheets to be identified (as indicated by the arrows) in figs. 1 (a) and (b). After careful inspection of the two sets of HRTEM images one may gain the qualitative impression that, if there is any observable difference between the two phases, it concerns only the perfection of individual  $CuO_2$  sheets, and the adjacent Tl-O layers. Fluctuations of intensity and image detail occur more frequently for the orthorhombic phase (fig. 1 (a)) than for the tetragonal phase (fig. 1 (b)).

One may conclude that the presence of varying densities of small defects in the  $CuO_2$  sheets, such as copper and/or oxygen vacancies, or the presence of thallium vacancies or Cu substituted for Tl on the adjacent Tl-O layers, would certainly lead to variable  $T_c$ . Further attempts to resolve this issue, by controlling the Tl/Cu ratio and the oxygen stoichiometry, are proceeding. HRTEM is expected to play a direct role in this study since it has the capability to reveal local fluctuations in short-range ordering within the  $CuO_2$  sheets.

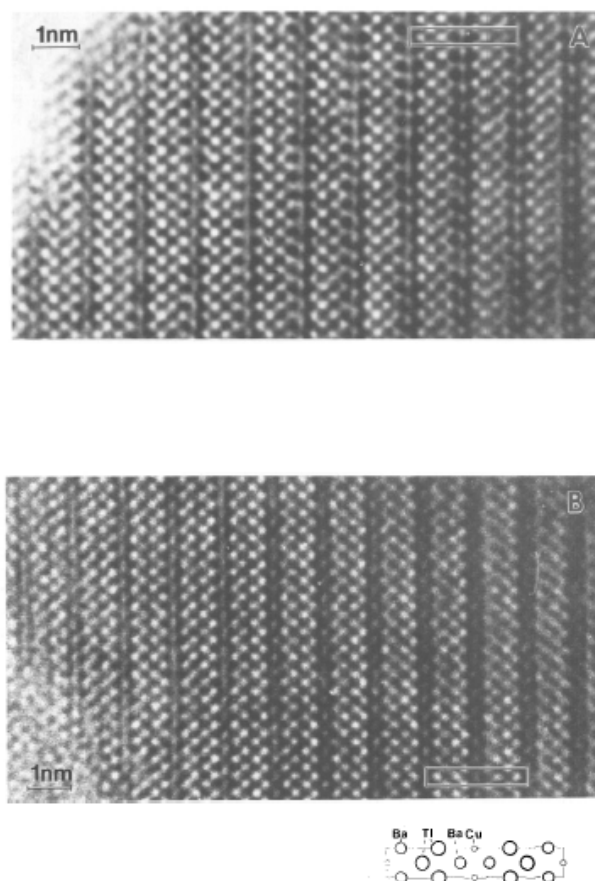


Fig. 1. HRTEM images of orthorhombic (a) and tetragonal (b)  $Tl_2Ba_2Cu_1O_{6+x}$ . The images are obtained under conditions where the atomic columns appear as black dots; the projection of the unit cell (outlined) does not match with the structural model.

### 4. X-ray, metallographic and microprobe investigations

The crystal structure was studied at ambient temperature by X-ray diffraction using

a Guinier camera with Cu K $\alpha$  radiation. Silicon was added to the powdered samples as an internal standard ( $a = 5.4308 \text{ \AA}$ ).

The lattice parameters of the  $Tl_2Ba_2Cu_1O_{6+x}$  orthorhombic and tetragonal phases were determined from least-squares fits using more than 20 lines ( $10^\circ < 4\theta < 160^\circ$ ). The lines were indexed according to the space group I4/mmm for the tetragonal phase [4,5] and Ccc2 (A2aa) for the orthorhombic phase [6]. The X-ray diffraction patterns of a tetragonal (12EA-0) and an orthorhombic (TKO-930) sample are presented in fig. 2. The lattice parameters are listed in table 1.

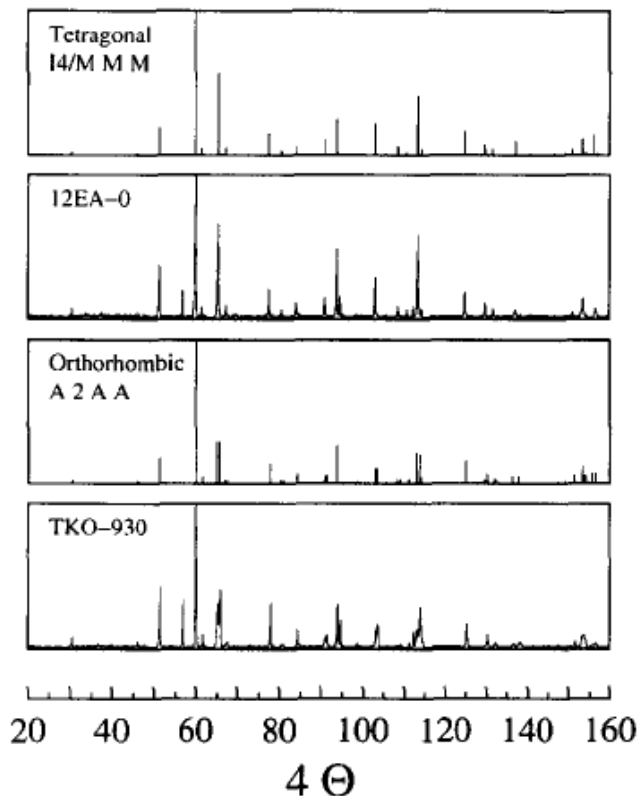


Fig. 2. Calculated and measured X-ray diffraction patterns for tetragonal (12EA-0) and orthorhombic (TKO-930) samples.

Microstructural investigations were carried out after polishing the samples using diamond paste. The surface was examined in a light microscope and in a scanning electron microscope (SEM, Cambridge Instruments Stereoscan 360). In the latter case, the polished samples were covered with a 6  $\text{\AA}$  thick silver layer. Energy dispersive analysis (EDAX) was performed on the M lines

of thallium, L lines of barium and K lines of copper by means of a Tracor Northern system. These investigations were corrected by a standard. The global stoichiometry of our samples was determined using plasma emission spectroscopy. Figure 3 shows optical micrographs of three tetragonal superconducting samples (TA2-850, TM-850 and THE-850) and one orthorhombic non-superconducting sample (TKO-930). Only 2201 grains can be seen in this figure. In the samples prepared using batch B, we observed in polarised light some yellow traces ( $< 5\%$  by volume) of starting  $Tl_2Ba_2O_5$  impurity phase and very small CuP grains ( $< 0.1\%$  by volume). Using batch A, only CuP and  $Ba_2Cu_3O_x$  impurities were detected (both  $< 0.1\%$  by volume). Figure 4 shows a SEM image of the TM-850 sample. The EDAX analyses, the plasma emission spectroscopy, the HREM investigations and the analysis of the impurity phases indicate in both the tetragonal and orthorhombic samples synthesised at high pressure that:

- (1) the global stoichiometry is  $Tl:Ba:Cu = 2:2:1$ . Consequently, the small mass loss during the synthesis has to be attributed to all metallic elements and also to the oxygen content in the preparation of the tetragonal phase;
- (2) we do not find a significant variation of the cation stoichiometry between the 2201 grains;
- (3) we do not observe cation vacancies in the 2201 structure;
- (4) depending on the initial batch, we observed a small difference in the ratio  $Tl/Cu$  between local and global analyses in our 90 K superconducting samples. This suggests a small homogeneity domain  $Tl_{1-x}Cu_x$  ( $0 \leq x \leq 0.1$ ). The superconducting properties and the change of structure can be attributed to the oxygen concentration alone. Note that under one atmosphere pressure, the tetragonal superconducting phase can only be obtained with a deficiency of thallium [1, 7, 8].

Table 1  
Parameters of the samples used

Sample	Batch	Gas preparation	$T_{c \text{ onset}}$ (K) <sup>a)</sup>	$f$ (%)	$D$	$\chi_0(T=0)$ ( $\times 10^{-8}$ emu/g)	wt. ppm Fe equiv.	$a$ (Å)	$b$ (Å)	$c$ (Å)
TH2-850	B	helium	90.8	56.3	0.14	-6.5	0	$a=b=3.8694(4)$		23.221(4)
THE-850	B	helium	91.8	49.2	0.11	-6.2	0	$a=b=3.8674(3)$		23.218(3)
TM-850	B	argon	91.1	43.9	0.12	-5.8	0	$a=b=3.8717(5)$		23.225(4)
TA2-850	A	argon	92.1	62.8	0.19	-	13.2	$a=b=3.8706(4)$		23.224(3)
TK2-R	A	argon	90.5	53.1	0.16	-	2.6	$a=b=3.8685(3)$		23.223(3)
12EA-0	A	argon	92.0	61.4	0.09	-	4.3	$a=b=3.8700(3)$		23.226(2)
12EA-11	A	argon	87.4	51.2	0.13	-	-	$a=b=3.8693(4)$		23.230(3)
TKO-930	A	oxygen	-	-	-	-	0	5.4467(8)	5.4911(7)	23.144(2)
12E-7	A	oxygen	-	-	-	-	-	5.4470(6)	5.4974(5)	23.141(2)

<sup>a)</sup> The onset is defined as 0.2% of ideal Meissner diamagnetism.

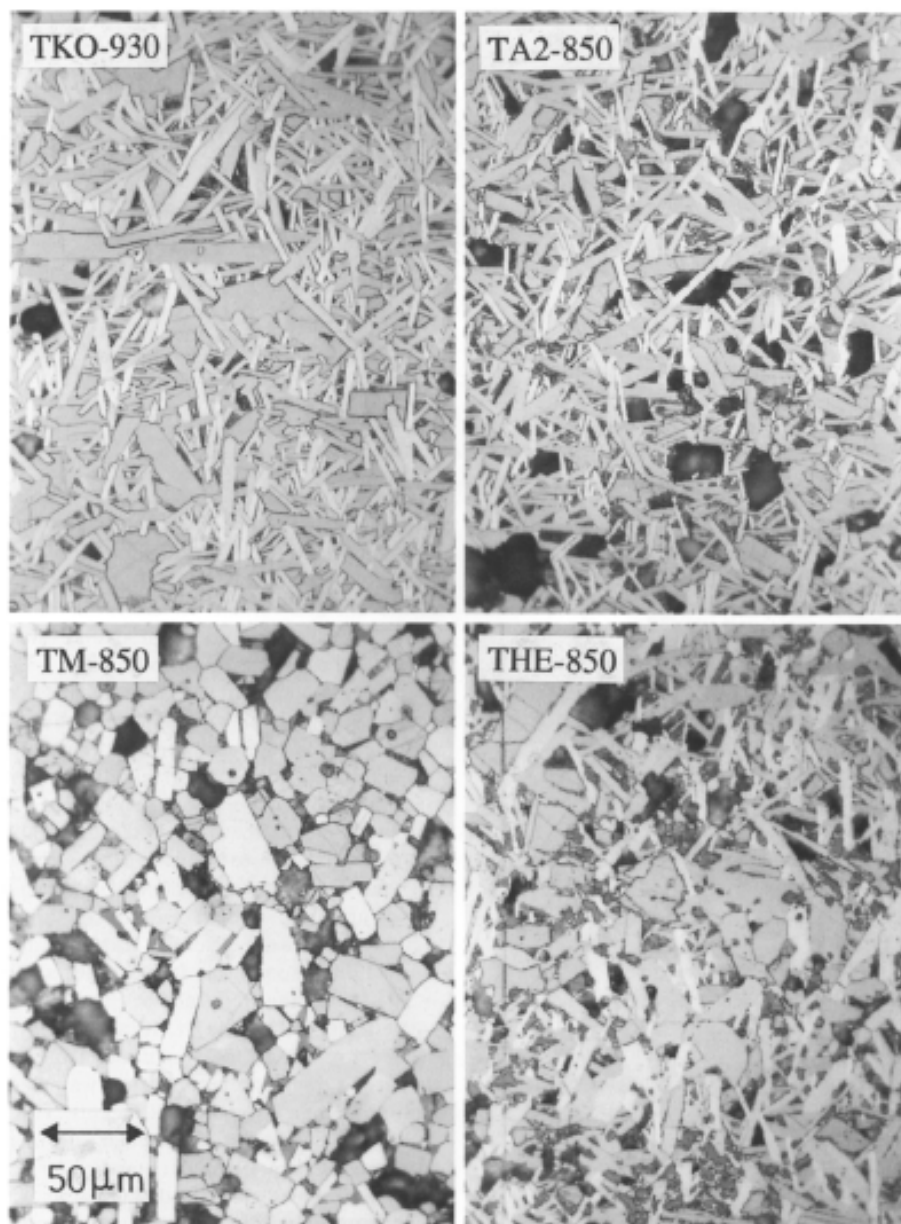


Fig. 3. Optical micrographs of one orthorhombic (TKO-930) and three tetragonal samples.

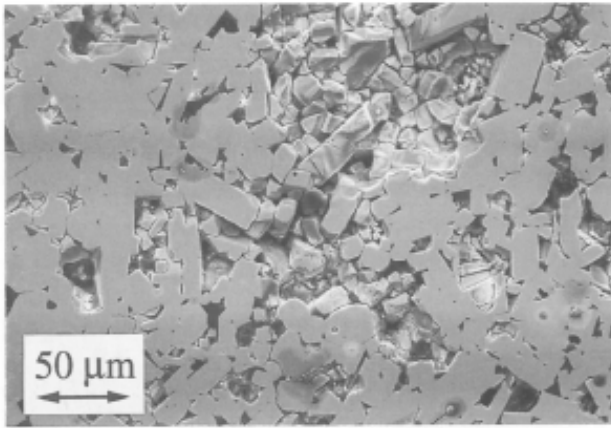


Fig. 4. SEM image of the TM-850 tetragonal sample.

## 5. AC susceptibility

The superconducting transitions were detected by means of a mutual inductance bridge operating between 80 and 800 Hz. The AC field amplitude was set in a first run to a low value of typically 0.05 Per ms. The earth field is compensated by a screen of  $\mu$ -metal. All curves show a double transition similar to the example shown in fig. 5. The low-temperature value of the susceptibility is equal to -1.72 (sample TH2-850) due to underestimation of the shielded volume. Actually, normalisation to the geometrical volume would give at low temperature a value of the susceptibility near -1.2 which corresponds closely to the expected value in the case of complete shielding with demagnetising effects taken into account. The upper transition at 90 K does not give rise to any appreciable dissipation at low field amplitude. Its shape does not depend on the amplitude or the frequency of the AC field, and its amplitude relative to full shielding is close to the Meissner fraction of the sample determined at a relatively high field strength of 20 Oe (see below). The second step between 60 and 80 K is accompanied by a broad dissipation peak. Its midpoint is shifted by +2.5K when the frequency of the AC field is increased from 80 to 800 Hz. Its shape and position depend strongly on the amplitude of the AC field; the second transition is completely washed out by a field amplitude larger than 20 Oe rms. This behaviour is characteristic of a granular superconductor with very weak intergranular

coupling [9]. The upper step close to 90 K gives the intragrain transition temperature. Between this temperature and approximately 80 K, the sample effectively behaves as a superconducting powder. The lower transition occurs when the critical current of the junctions between the superconducting grains exceeds the order of magnitude  $H/R$ , where  $R$  is the radius of the sample. The latter ratio amounts to only  $0.5 \text{ A/cm}^2$ , i.e. orders of magnitude below values typical of  $\text{YBa}_2\text{Cu}_3\text{O}_7$  close to  $T_c$ . Inter-grain links are therefore particularly weak in the 2201 material, although the reason is unclear. A similar behaviour was observed in the related family of  $\text{Bi}_2\text{Sr}_2\text{CaCu}_2\text{O}_{8+x}$  ceramics [10]. On the other hand, an intra-granular dissipation peak grows with the AC field amplitude being increased (see inset of fig. 5). The growth of this dissipation peak is due to the fact that the bulk of the grains is becoming effectively probed as the AC field amplitude is increased and the screening by the surface barriers is no more efficient during the major part of the AC ripple [11].

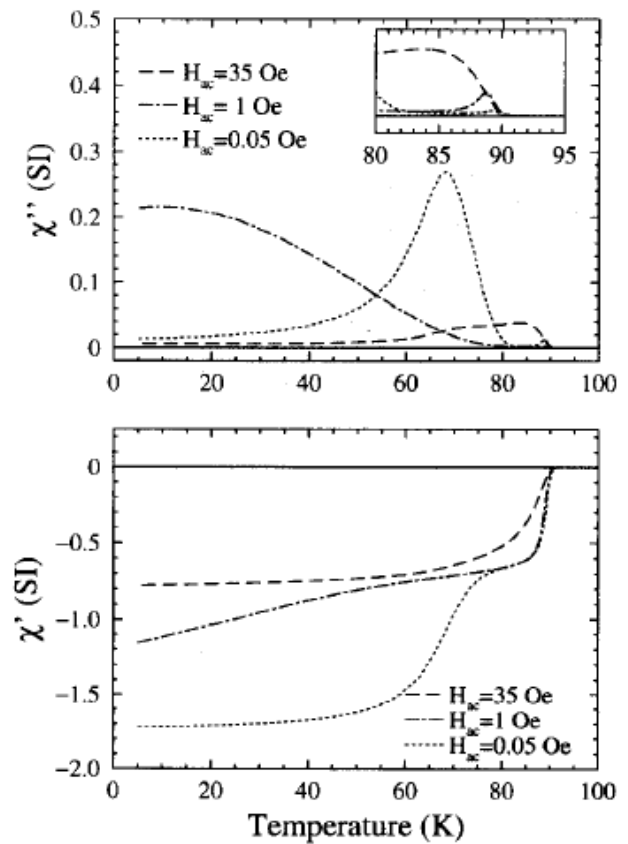


Fig. 5. AC susceptibility of sample TH2-850 at three levels of excitation: 35, 1 and 0.05 Oe. Upper graph: imaginary part; lower graph: real part.

### 6. DC field effect: the irreversibility line

Due to their large anisotropy, the Tl-based compounds, as the Bi-based family, show large domains of reversibility in the (H, T) plane. The determination of the frontier-line or irreversibility line  $H^*(T)$ , although the experimental and theoretical criteria for its definition are still controversial, presents some interest for the classification of these materials as far as critical current promises are concerned. In the case of the present  $Tl_2Ba_2Cu_1O_{6+x}$ , we determined the  $H^*(T)$  by measuring the AC susceptibility under a DC magnetic field. The apparent huge shift of the onset temperature (see fig. 6  $-\chi' < 0$ ) is due to the fact that in the reversible regime  $\chi'$  has a positive weak value which on the scale of the whole transition could not be distinguished from null value. Thus the onset temperature of  $\chi' < 0$  does not correspond to a  $T_c(H)$  critical temperature but rather to the departure from reversibility [ 12 ].

The irreversibility line determined by this criterion is shown on fig. 7. Although a  $H^{1/3}$  power law appears to be approximately obeyed, no simple power law can be established as in the case of other high- $T_c$  compounds. This fact may be due to the polycrystalline character of the samples and thus to the angular dependence of  $H^*(T)$ .

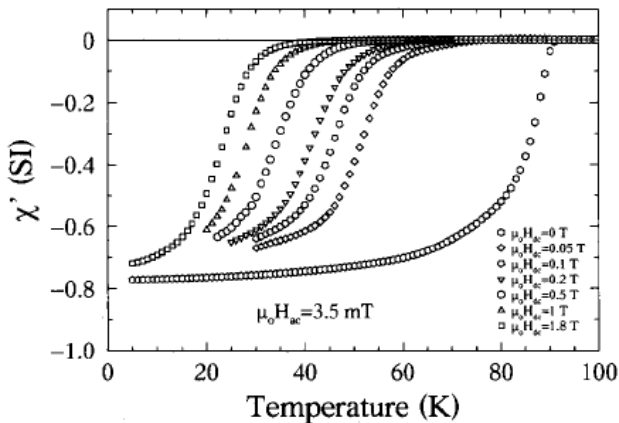


Fig. 6. AC susceptibility of sample TH2-850 in different DC magnetic fields.

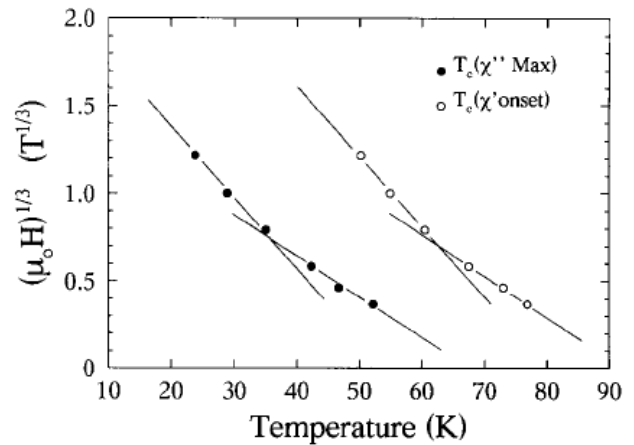


Fig. 7.  $T_c(\chi'_{max})$  and  $T_c(\chi'_{onset})$  vs.  $H^{1/3}$ .

### 7. Meissner effect

In these measurements, we use the c.g.s. system where  $B=H+4\pi M$  and  $\chi_v=M/H=\rho\chi_g$ . The Meissner effect (field cooling) was measured using a RF SQUID magnetometer with an external magnetic field of 20 Oe. The Meissner flux expulsion ratio  $f = -4\pi\chi_v$  was evaluated using an effective sample volume given by  $m/\rho$ , where  $m$  is the sample mass and  $\rho$  the X-ray density ( $\rho = 8.0 \text{ g/cm}^3$ ). A geometric demagnetisation factor  $D=0.11-0.19$ , depending on the sample shape, was taken into account. The corrected susceptibility reads  $\chi_g = \chi_g^m / (1 - 4\pi D\rho\chi_g^m)$ , where  $\chi_g^m$  is the measured susceptibility. The external magnetic field was calibrated using a high-purity Pb sphere in the superconducting state.

Figure 8 shows the Meissner flux expulsion for four tetragonal samples. The sharpness of the transitions at 90-92 K (onset) denotes the homogeneity of the oxygen concentration. The low-temperature tail follows the behaviour predicted for a granular sample with  $R/\lambda(0) \sim 30$ , where  $R$  is the radius of the superconducting grains and  $2\lambda(0)$  is the penetration depth at  $T=0K$  [ 13 ]. This ratio is consistent with the usual values of  $\lambda(0)$  in high-temperature superconductors and with the average grain size observed in optical micrographs. An analysis of the effective superconducting volume is given elsewhere [ 5 ].

No superconducting signal was observed down

to 6K in the oxidised orthorhombic phase (sample TKO-930, not shown).

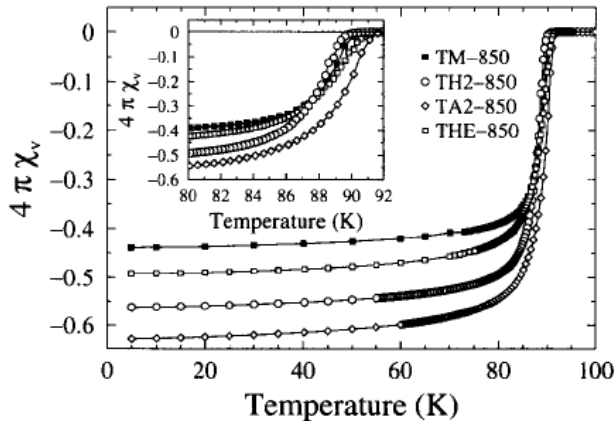


Fig. 8. Field cooling susceptibility (Meissner effect) at  $H = 20$  Oe. Ideal diamagnetism corresponds to  $4g\chi_g = -1$  in these units. Inset: expanded scale. The low-temperature tail is consistent with a grain size to penetration depth ratio of about 30.

## 8. Normal-state susceptibility

The normal-state susceptibility was measured using

the same magnetometer with an external magnetic field of 20 kOe. No significant amount of ferromagnetic impurities was detected by means of Honda's method [14] in batch A used for samples TH2-850, THE-850 and TM-850 (see table 1). Figure 9 shows the normal-state susceptibility of three tetragonal samples (TM-850 and TA2-850 prepared under argon, TH2-850 prepared under helium). The slight Curie-Weiss behaviour of sample TA2-850 is due to the presence of a small amount of  $\text{BaCuO}_2$  impurity phase. This sample does not contain any residual  $\text{Tl}_2\text{Ba}_2\text{O}_5$  precursor. On the contrary, samples TM-850 and TH2-850 contain no  $\text{BaCuO}_2$ , but a small amount of  $\text{Tl}_2\text{Ba}_2\text{O}_5$ , which was observed at the limit of detection of X-ray and micrographic techniques. The susceptibility of the pure precursor  $\text{Tl}_2\text{Ba}_2\text{O}_5$  is also presented in fig. 9. It remains diamagnetic and almost constant from 100 to 400 K.

The presence of this unreacted precursor results in a small downward shift of the total susceptibility with respect to the intrinsic

contribution of the  $\text{Tl}_2\text{Ba}_2\text{CuO}_6$  phase. We note that both the susceptibility of sample TA2-850 corrected for the Curie contribution, and the susceptibility of samples TM-850 and TH2-850 corrected for  $\text{TlBa}_2\text{O}_5$ , can be brought into coincidence if the concentration of the latter impurity is  $\sim 5\%$  by volume. The resulting intrinsic susceptibility of  $\text{Tl}_2\text{Ba}_2\text{CuO}_6$  is shown as a full line in fig. 9. It is small, diamagnetic, and essentially constant above 150 K.

For a number of oxide superconductors where the transition temperature  $T_c$  can be varied appreciably with different hole doping, e.g.  $\text{La}_{2-x}\text{Sr}_x\text{CuO}_{4-y}$  [15-17],  $\text{YBa}_2\text{Cu}_3\text{O}_{7-d}$  [18,19],  $\text{Tl}_2\text{Ba}_2\text{CuO}_{6+x}$  [20],  $\text{Bi}_2\text{Sr}_2\text{CaCu}_2\text{O}_{8+x}$  [10],  $\text{Y}_2\text{Ba}_4\text{Cu}_7\text{O}_{15+z}$  [21], an interesting empirical correlation emerges between  $T_c$  and the normal-state magnetic susceptibility. At the hole doping that maximises  $T_c$ , the normal-state susceptibility tends to become temperature independent. Above (or below) the optimum, the slope  $\delta\chi_g/\delta T$  is negative (or positive), respectively. The intrinsic normal-state susceptibility of  $\text{Tl}_2\text{Ba}_2\text{CuO}_6$  above the region of superconducting fluctuations is remarkably temperature independent (see fig. 9). By analogy with the systems mentioned above, it can be concluded that samples superconducting at 90 K are close to the optimum hole doping. We note, however, that a recent publication reports superconductivity up to 110 K in some  $\text{Tl}_{1.85}\text{Ba}_2\text{Cu}_{1.15}\text{O}_6$  crystals [22]. This point deserves further investigation.

The diamagnetic core susceptibility of  $\text{Tl}_2\text{Ba}_2\text{CuO}_6$  is  $-2.29 \times 10^{-7} \text{emu/g}$  if we assume that the oxidation states of the elements are  $\text{Tl}^{+3}\text{Ba}^{+2}\text{Cu}^{+2}$  [23]. This value normalised to one mole is similar to those of the superconducting phases in the  $\text{YBaCuO}$  system,  $\text{YBa}_2\text{Cu}_3\text{O}_{7-d}$ ,  $\text{YBa}_2\text{Cu}_{3.5}\text{O}_{7.5+d}$  and  $\text{YBa}_2\text{Cu}_4\text{O}_8$  [24]. In contrast to the latter, the 2201 phase of the  $\text{TlBaCaCuO}$  system has but one copper atom per formula unit to overcome the core diamagnetism by the Pauli and orbital contributions. This fact probably explains why the total magnetic susceptibility is negative. The total susceptibility  $\chi_o(T=0)$  extrapolated from above 120 K is  $-5 \times 10^{-8} \text{emu/g}$ , or

$-4 \times 10^{-5}$  emu/mole Cu. These values include a correction of  $1 \times 10^{-8}$  emu/g or  $1 \times 10^{-5}$  emu/mole Cu for the  $Tl_2Ba_2O_5$  impurity. Our results are in fair agreement with those of Allgeier et al. [20]. The sum of the Pauli and van Vleck contributions amounts to  $1.54 \times 10^{-4}$  emu/mole Cu, to be compared with  $1.6 \times 10^{-4}$  / mole Cu for  $YBa_2Cu_3O_7$  [24].

The rounding  $\chi_g(T)$  just above  $T_c$  is attributed to superconducting fluctuations. The leading term of the Gaussian fluctuation contribution can generally be written as  $\chi_{fl}(T) = -A\tau^\alpha$  where  $\tau = |1 - T/T_c|$ . Unexpectedly, the exponent  $\alpha$  that best fits the incipient diamagnetism is neither -0.5 nor -1, as would be expected for 3D or 2D fluctuations, respectively, but -2. The meaning of this observation is still unclear.

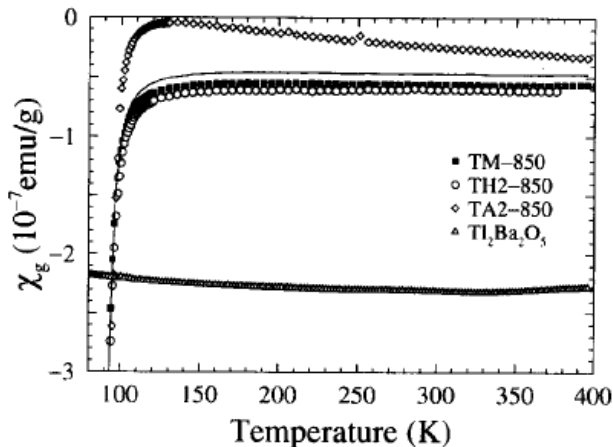


Fig. 9. Normal-state susceptibility vs. temperature at  $H = 20$  kOe for three tetragonal samples. The lowest curve shows the susceptibility of the precursor  $Tl_2Ba_2O_5$ . See text.

## 9. Hysteresis measurements and critical currents

Using the SQUID magnetometer, we also measured the magnetic hysteresis at 5 and 77 K (see fig. 10). The measurements of  $M(H)$  were taken after zero-field cooling from above  $T_0$ . The complete re-versibility at 77 K, almost 15 K below  $T_0$ , is unusual. In terms of the "irreversibility line" concept,  $Tl_2Ba_2CuO_6$  is more closely related to  $Bi_2Sr_2CaCu_2O_8$  than to  $YBa_2Cu_3O_7$ .

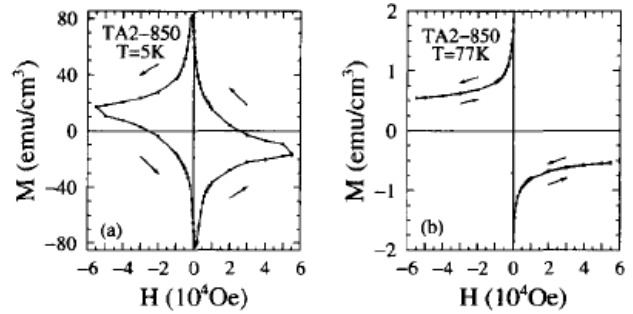


Fig. 10. Magnetization cycles at (a) 5 K and (b) 77 K.

The critical current is evaluated on the basis of Bean's critical model [25,26]:

$$j_c \sim -3 (M^+(H) - M^-(H)) / \varnothing,$$

where  $j_c$  is the critical current,  $M^+(H)$  and  $M^-(H)$  are the magnetisations measured with increasing and decreasing magnetic field, respectively, and  $\varnothing$  is the diameter of the cylinder perpendicular to the field (in usual units  $A/cm^2$ ,  $emu/cm^3$ , and  $cm$ ):  $j_c \sim -30 \{M^+(H) - M^-(H)\} / \varnothing$ .

Using the sample diameter for  $\varnothing$ , we obtain a macroscopic critical current density of about  $8 \times 10^3 A/cm^2$  at 1 T and 5 K. Using rather the typical grain size of 5  $\mu m$ , consistent with optical micrographs and with the shape of Meissner curves, we obtain  $j_c = 1.6 \times 10^6 A/cm^2$ , a value that is more characteristic of intragranular critical current densities. At 77 K and 1 T, the absence of any hysteresis only gives an upper limit of 12  $A/cm^2$  for the macroscopic critical current density. This rough analysis is only expected to yield relative indications.

## 10. Specific heat

The calorimeter used for this study is of the adiabatic, continuous heating type; the sample is in vacuo. Years of operation have confirmed an accuracy better than 1% using 0.5g samples, whereas the scatter may be as low as 0.1 to 0.2%. Three samples were selected for the specific heat experiments in the temperature range 30-300 K (table 1). Sample TA2-850 was synthesised in high-pressure argon, whereas sample THE-850 was synthesised in high-pressure helium. Both have identical  $T_{c0}$ s close to 90 K, as shown by the Meissner curves (see

fig. 8). The specific heat curve of sample 12EA11 prepared in argon ( $T_c=84.5\text{K}$ , Meissner midpoint), not shown, is similar to that of TA2-850.

A giant peak was observed at  $83.74\text{K}$  for those samples which were prepared under argon (see fig. 11), somewhat reminiscent of Butera's unusual results on  $\text{YBa}_2\text{Cu}_3\text{O}_7$  [27].

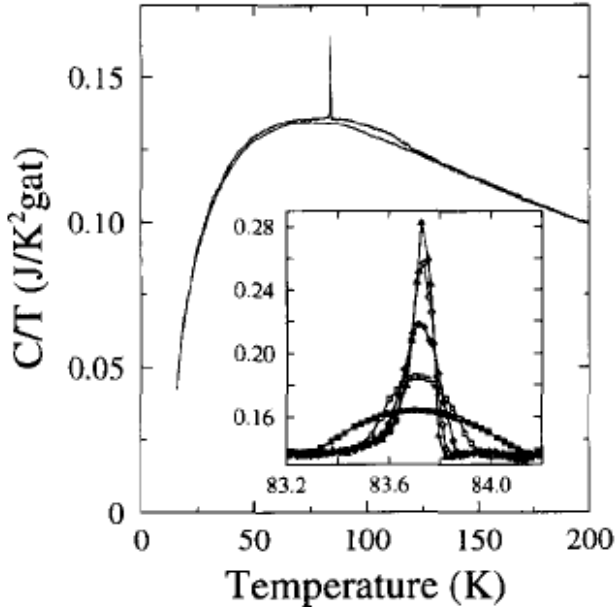


Fig. 11. Specific heat  $C/T$  vs. temperature for sample TA2-850 prepared under Ar protective atmosphere (upper curve), and sample THE-850 prepared under He (lower curve). Inset: enlargement of the Ar peak at  $83.74\text{K}$ , sample TA2-850, using progressively smaller temperature intervals to determine the "instantaneous" specific heat, from  $0.8\text{K}$  (lowest curve) to  $0.4$ ,  $0.2$ ,  $0.1$  and  $0.05\text{K}$  (uppermost curve).

Emphasizing the resolution at the expense of an increased scatter, we find that the width of the peak at half-height is close to  $0.1\text{K}$ , while the amplitude exceeds the baseline specific heat by  $\sim 100\%$  (fig. 11, inset). This peak almost coincides with  $T_c$  for sample 12EA11, but experiments with the higher- $T_c$  sample TA2-850 on the one hand, and with the argon-free sample THE-850 on the other hand, clearly demonstrate that this anomaly has nothing to do with superconductivity. It is merely due to the melting of minute amounts of argon gas trapped

in pores. Let us recall that the triple point of Ar, a fixed point of the ITS-90 temperature scale [28], is given by  $T=83.8058\text{K}$  and  $p=0.68\text{bar}$ , whereas its critical point lies at  $150.9\text{K}$  and  $48\text{bar}$ . The integrated latent heat indicates that sample TA2-850, weighing  $0.61\text{g}$ , contains  $170\mu\text{g}$  of argon. The evaporation of argon also gives rise to an excess specific heat extending up to  $130\text{K}$ , but decreasing strongly beyond  $110\text{K}$  (fig. 11). This reflects a distribution of gas pressures in the pores, with a typical value of  $20\text{bar}$  at room temperature. The closed pores represent then  $6\%$  of the sample volume, to be compared with a total porosity of about  $30\%$ . The extrapolated pressure in the pores is  $70\text{bar}$  at  $850^\circ\text{C}$ . Pores are therefore sealed at high temperatures during the heat treatment rather than during cooling under constant external pressure. This effective sealing may severely limit diffusion in the bulk if one subsequently attempts to oxidise the sample (e.g. to induce a tetragonal to orthorhombic phase conversion).

The superconducting transition is not easily distinguished from these extrinsic features in the samples prepared under argon gas. We therefore turn to the sample prepared in helium for a further analysis (fig. 11, lower curve).

Figure 12 shows an enlargement of the transition region. The  $C/T$  scale is expanded to show  $5\%$  of the total specific heat at  $T_0+20\text{K}$ . No mean-field step is observed, but a smeared break in the slope is noticeable. Such a change in the slope cannot be accounted for by any positive phonon distribution. It is clearly due to the condensation of electrons. We attempted to fit the data over a wide region using the following model. The phonon density-of-states is represented by three Einstein peaks located at energies  $\omega_0$ ,  $\omega_1$  and  $\omega_2$ ; their weights are  $D_0$ ,  $D_1$ , and  $D_2$ .

The electronic mean-field specific heat is represented by the two-fluid model, with  $C_{mf}^- = 3\gamma T^3/T_c^2$  for  $T < T_c$  and  $C_{mf}^+ = \gamma T$  for  $T > T_c$ . Anticipating the result, we mention that this term will be insignificantly small, as expected from the absence of any observable specific heat jump. The choice of the two-fluid model is therefore not critical. The superconducting fluctuations are represented by

a contribution derived from the Lawrence-Doniach model [29], expressing the smooth crossover from 3D Gaussian fluctuations close to  $T_c$  to 2D Gaussian fluctuations farther away from  $T_c$ :

$$C_{\bar{n}} = \frac{k_B}{8\pi V_c \sqrt{(\tau d/2\xi_c)^2 + \tau/2}}, \quad T < T_c,$$

$$C_{\bar{n}}^{\dagger} = \frac{k_B}{8\pi V_c \sqrt{(\tau d/2\xi_c)^2 + \tau}}, \quad T > T_c;$$

$C_{\bar{n}}$  is the fluctuation specific heat in  $\text{J}/\text{cm}^3\text{K}$ ,  $V_c = \xi_{ab}^2 \cdot \xi_c$  is the coherence volume,  $\xi_{ab}$  and  $\xi_c$  are the coherence lengths in the (a, b) plane and along the c-axis, respectively;  $\tau = |1 - T/T_c|$  is the reduced temperature, and  $d$  is the interlayer distance. The leading power of  $\tau$  close to  $T_c$  is  $-1/2$ , and the term containing  $d/2\xi_c$  may be omitted with practically unchanged results. The parameters  $\omega_0, \omega_1, \omega_2, D_0, D_1, D_2, \gamma, T_c$  and  $V_c$  are refined simultaneously using 700 data between 40 and 230 K. The region 90 to 93 K is omitted. The result for all parameters is stable with respect to the starting point of the least-squares fit program. The residual standard deviation is 0.15%.

Concerning the phonon spectrum, we only mention that the  $\omega$ s thus found lie within the range of expected phonon frequencies (106, 296 and 670K), and that their total weight comes out as 1.04 times  $3N$  modes per gram-atom, a reasonable result. The fit determines three other parameters: the specific heat jump,  $0.4 \text{ mJ}/(\text{K}^2 \text{mole formula unit})$ , which is insignificantly small, the critical temperature  $T_c = 91.8\text{K}$ , and an average coherence length  $(\xi_{ab}^2 \cdot \xi_c)^{1/3} = 7.5 \text{ \AA}$ . Using a similar analysis, we found  $(\xi_{ab}^2 \cdot \xi_c)^{1/3} = 6.4$  to  $6.5 \text{ \AA}$  both for  $\text{YBa}_2\text{Cu}_3\text{O}_7$  and  $\text{Bi}_2\text{Sr}_2\text{CaCu}_2\text{O}_8$  [30]. Figure 12 (inset) shows the total specific heat minus the fitted phonon contribution. The anomaly at  $T_c$  never exceeds 0.9% of the total specific heat. Let us mention, however, that the accuracy of such an analysis including the lattice specific heat given by a fitted phonon spectrum could be assessed in the system  $\text{Bi}_2\text{Sr}_2\text{CaCu}_2\text{O}_{8+y}$ , where  $T_c$  could be alternatively suppressed by a

suitable heat treatment [31].

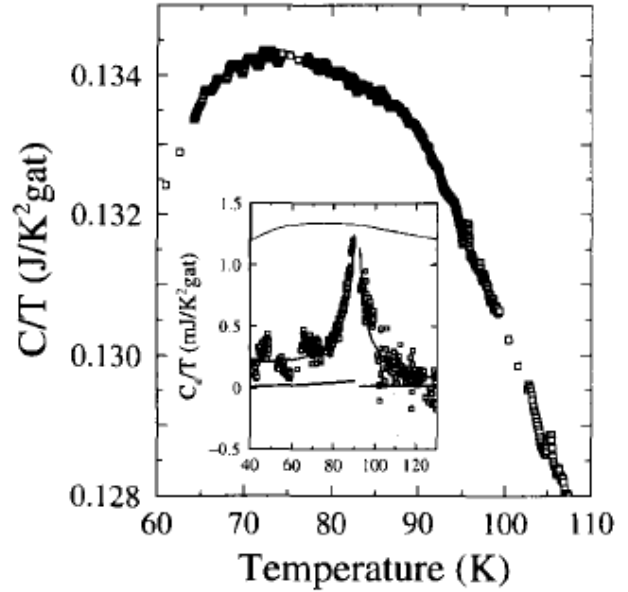


Fig. 12. Total specific heat  $C/T$  vs. temperature for sample THE-850, expanded scale in the vicinity of  $T_c = 91.8 \text{ K}$ . Inset: electron specific heat (total specific heat minus fitted lattice specific heat)  $C_e/T$  in the vicinity of  $T_c$ . The uppermost curve shows 1% of the total specific heat. The curve passing through the data is the fitted function including both 3D/2D Gaussian fluctuations and a small mean-field jump. The latter is negligibly small, as shown separately by the lowest curve.

The most intriguing feature is the absence of any well-developed mean-field specific heat jump at  $T_c$ . Smearing by inhomogeneities is not a very satisfactory explanation, since the homogeneity, grain size, Meissner effect, etc. compare favourably with those of  $\text{YBa}_2\text{Cu}_3\text{O}_7$  samples which show a clear-cut jump. One may speculate that the electron density-of-states at the Fermi level is extremely small, and/or that the transition at 90K does not result in long-range coherence.

Let us mention here that granularity at the  $5 \mu\text{m}$  scale can hardly explain the loss of the specific heat jump. Generally speaking, granularity may suppress the jump by reducing the effective dimensionality to zero. The relevant parameter characterizing the shift from the mean-field result is the ratio of the average single-electron level spacing to the thermal energy,  $\delta = 1/N(O) \Omega k_B T_c$ ;  $N(O)$  is the single-spin energy

density-of-states per unit volume, and  $\Omega$  is the small particle volume. For  $\delta = 0.1$  to 1, the specific heat jump at  $T_c$  is washed out [32]. Even using the extremely low Sommerfeld constant given by the fit, sizeable effects would require a particle size of 100 Å or less in  $Tl_2Ba_2CuO_6$ .

## 11. Conclusion

Starting with the  $Tl_2Ba_2O_5$  precursor and CuO, we have shown that the tetragonal  $Tl_2Ba_2CuO_{6+x}$  superconducting phase with  $T_c=90$  K can easily be synthesised using a high pressure (100 bar) of argon or helium at 850°C. The high pressure effectively prevents the thallium evaporation. The orthorhombic non-superconducting phase is synthesised at 930 °C under 100 bar of oxygen. Synthesised at high pressure, we found that the cation stoichiometry of these two phases is the same. HRTEM investigations indicate no metallic element vacancies, but we do not exclude some homogeneity domain  $Tl_{1-x}Cu_x$ .

The superconducting transitions of our tetragonal samples are sharp and present a substantial Meissner effect at low temperature (60%). The AC susceptibility at low field shows distinct intra- (90 K) and inter-grain transitions. The latter are due to the bad coupling between the superconducting grains (weaklink structure). At larger excitation field, the second transition disappears. AC susceptibility measurements under a DC magnetic field show a large reversibility domain in the (H, T) plane. Magnetisation measurements at constant temperature ( $M(H)_T$ ) indicate no significant hysteresis suggesting very low pinning and consequently a low intergrain critical current density. Investigation of the normal state susceptibility shows no intrinsic Curie-Weiss behaviour and a temperature independence in the region where the superconducting fluctuations no longer contribute. By analogy with other high- $T_c$  systems, this fact suggests that we are at the optimum hole doping for maximum superconducting critical temperature. Although the specific heat measurements show

an anomaly at  $T_c$  which can be accounted for in terms of fluctuations with a Lawrence-Doniach coupled layer model, the mean-field specific heat jump which can be deduced from our analysis is negligibly small.

## Acknowledgements

The authors are grateful to J.A. Fernandez, F. Liniger, F. Monnier, A. Naula and K. Wang for their technical assistance. This work was supported partially by the program EURODOC and the Fonds National Suisse de la Recherche Scientifique.

## References

- [1] J.-L. Jorda, T.K. Jondo, R. Abraham, M.T. Cohen-Adad, C. Opagiste, M. Couach, A.F. Khoder and F. Sibieude, Physica C205 (1993) 177.
- [2] T.K. Jondo, R. Abraham, M.T. Cohen-Adad and J.-L. Jorda, J. Alloys Compounds 186 (1992) 347.
- [3] L.A. Bursill, O. Leckel and M.G. Blanchin, J. Alloys Compounds, E-MRS Strasbourg, 1992, to be published.
- [4] Y. Shimakawa, Y. Kubo, T. Manako, H. Igarashi, F. Izumi and H. Asano, Phys. Rev. B 42 (1990) 10165.
- [5] C. Opagiste, M. Couach, A.F. Khoder, R. Abraham, T.K. Jondo, J.-L. Jorda, M.Th. Cohen-Adad, A. Junod, G. Triscone and J. Muller, J. Alloys Compounds, E-MRS Strasbourg, 1992, to be published.
- [6] A.W. Hewat, P. Border, J.J. Capponi, C. Chaillout, J. Chenevas, M. Godinho, E.A. Hewat, J.L. Hodeau and M. Marezio, Physica C 156 (1988) 369.
- [7] J.B. Goodenough and A. Manthiram, J. Solid State Chem. 88 (1990) 115.
- [8] A. Manthiram, M. Paranthaman and J.B. Goodenough, Physica C 171 (1990) 135.
- [9] K.-H. Müller, Physica C 159 (1989) 717.
- [10] G. Triscone, J.-Y. Genoud, T. Graf, A. Junod and J. Muller, Physica C 176 (1991) 247.
- [11] A.F. Khoder and M. Couach, in: Magnetic Susceptibility of Superconductors and other Spin Systems (1992).
- [12] A.F. Khoder, M. Couach and J.Y. Henry, Europhys. Lett. 15 (1991) 337.

- [13] J.R. Clem and G. Kogan, Jpn. J. Appl. Phys. 26-3 (1987) 1161.
- [14] K. Honda, Ann. Phys. 32 (1910) 1027.
- [15] D.C. Johnston, Phys. Rev. Lett. 62 (1989) 957.
- [16] D.C. Johnston, J. Magn. Magn. Mater. 100 (1991) 218.
- [17] J.B. Torrance, A. Bezing, A.I. Nazzari, T.C. Huang, S.S.P. Parkin, D.T. Keane, S.J. LaPlaca, P.M. Horn and G.A. Held, Phys. Rev. B 40 (1989) 8872.
- [18] T. Kawagoe, T. Mizoguchi, K. Kanoda, T. Takahashi, M. Hasumi and S. Kagoshima, J. Phys. Soc. Jpn. 57 (1988) 2272.
- [19] G. Triscone, J.-Y. Genoud, T. Graf, A. Junod, J. Muller, J. Alloys Compounds, E-MRS Strasbourg, 1992, to be published.
- [20] C. Allgeier and J.S. Schilling, Physica C 168 (1990) 499.
- [21] G. Triscone, J.-Y. Genoud, T. Graf, A. Junod and J. Muller, Physica C 201 (1992) 1.
- [22] N.N. Kolesnikov et al., Physica C 195 (1992) 219.
- [23] Konig's tables, Landolt-Börnstein, New Series, Vol. 11/2, 16 (Springer, Berlin/New York, 1966).
- [24] J.-Y. Genoud, T. Graf, A. Junod, G. Triscone and J. Muller, Physica C 185-189 (1991) 597.
- [25] C.P. Bean, Rev. Mod. Phys. 36 (1964) 31.
- [26] W.A. Fietz and W.W. Webb, Phys. Rev. 178 (1969) 657.
- [27] R.A. Butera, Phys. Rev. B 37 (1988) 5909.
- [28] H. Preston-Thomas, Metrologia 27 (1990) 3.
- [29] L.N. Bulaevskii, V.L. Ginzburg and A.A. Sobyanin, Physica C 152 (1988) 378; *ibid.*, 156 (1988) 652.
- [30] A. Junod, to be published.
- [31] A. Junod, to be published.
- [32] B. Mühlischlegel, D.J. Scalapino and R. Denton, Phys. Rev. B6 (1972) 1767.